







MHz-repetition-rate, sub-mW, multi-octave THz wave generation in HMQ-TMS

TOBIAS OLAF BUCHMANN,^{1,5}  EDMUND J. R. KELLEHER,¹ 
KORBINIAN J. KALTENECKER,¹ BINBIN ZHOU,¹  SEUNG-HEON
LEE,² O-PIL KWON,² MOJCA JAZBINSEK,³  FABIAN ROTERMUND,⁴
AND PETER UHD JEPSEN^{1,6}

¹DTU Fotonik, Technical University of Denmark, Ørsteds Plads 343, 2800 Kgs. Lyngby, Denmark

²Department of Molecular Science & Technology, Ajou University, 443-749 Suwon, South Korea

³Institute of Computational Physics, Zurich University of Applied Sciences, Technikumstrasse 9, 8400 Winterthur, Switzerland

⁴Department of Physics, Korea Advanced Institute of Science & Technology (KAIST), 34141 Daejeon, South Korea

⁵toobu@fotonik.dtu.dk

⁶puje@fotonik.dtu.dk

Abstract: We demonstrate the first megahertz (MHz) repetition-rate, broadband terahertz (THz) source based on optical rectification in the organic crystal HMQ-TMS driven by a femtosecond Yb:fibre laser. Pumping at 1035 nm with 30 fs pulses, we achieve few-cycle THz emission with a smooth multi-octave spectrum that extends up to 6 THz at -30 dB, with conversion efficiencies reaching 10^{-4} and an average output power of up to 0.38 mW. We assess the thermal damage limit of the crystal and conclude a maximum fluence of $\sim 1.8 \text{ mJ}\cdot\text{cm}^{-2}$ at 10 MHz with a $1/e^2$ pump beam diameter of 0.10 mm. We compare the performance of HMQ-TMS with the prototypical inorganic crystal gallium phosphide (GaP), yielding a tenfold electric field increase with a peak on-axis field strength of $7 \text{ kV}\cdot\text{cm}^{-1}$ and almost double the THz bandwidth. Our results further demonstrate the suitability of organic crystals in combination with fibre lasers for repetition-rate scaling of broadband, high-power THz sources for time-domain spectroscopic applications.

© 2020 Optical Society of America under the terms of the [OSA Open Access Publishing Agreement](#)

1. Introduction

Terahertz (THz) radiation is useful for a variety of applications covering the medical, security and scientific fields. The non-ionising properties combined with the transparency of many materials to THz frequencies make it a suitable imaging alternative to X-rays [1]; in addition, many molecules have multiple characteristic absorption bands within the THz spectral range, allowing for precise spectroscopy [2]. Furthermore, time-domain methods (*e.g.* THz TDS), sensitive to both the wave amplitude and phase, can provide more information on the material properties compared to conventional Fourier-transform spectroscopy schemes [3]. Common to all these applications is the requirement for a stable, short-pulse, and broadband THz source. There are four principal laser-based THz generation approaches: photo-conductive switching [4], laser-driven gas ionisation [5], emission based on spin-currents in metal structures (known as ‘spintronics’ [6]), and optical rectification (OR) [7]. With the development and commercial availability of high-power fibre-based laser sources with repetition-rates in the MHz range, OR is becoming a promising technique to generate high repetition-rate, high average-power THz radiation. Compared to high-energy kHz sources that often form the core technology of many spectroscopy laboratories, MHz repetition-rates support reduced measurement times and engender an inherently larger signal-to-noise ratio (SNR) due to the increased shot-rate within a given measurement interval. A commonly used crystal that is suitably phase-matched for OR at near-infrared (near-IR) wavelengths around 1035 nm is gallium phosphide (GaP). Successful

OR for THz wave generation with GaP at MHz repetition-rates with record output powers up to 300 μW driven by a Yb:fibre laser [8], and 1.35 mW driven by a thin-disk laser [9], has been demonstrated. In addition, large spectral bandwidths up to 8 THz at high repetition-rates up to 80 MHz have been achieved [10,11]. However, THz wave generation in GaP is limited to conversion efficiencies on the order of 10^{-6} - 10^{-5} . Significantly larger conversion efficiencies with MHz fibre sources are currently only achieved with a more complex tilted pulse front method with LiNbO_3 as the optical medium [12].

Organic crystals such as DAST or DSTMS possess a significantly larger second-order nonlinear coefficient than inorganic crystals (such as GaP), enhancing the conversion efficiency through OR for the THz wave generation process [13]. These specific crystals, however, are phase-matched at wavelengths longer than 1200 nm and are thus not compatible with existing high-power femtosecond fibre laser technologies that are predominantly based on ytterbium, with a gain bandwidth covering the region between 1020-1070 nm. To leverage existing MHz sources in the near-IR with an appropriate medium that can be phase-matched, we use the organic crystal HMQ-TMS, which was first reported for THz wave generation through OR in 2013 with 800 nm pump pulses at 1 kHz [14]. At this wavelength (of 800 nm), HMQ-TMS has shown a twenty-fold increase in the generated pulse energy compared to the inorganic nonlinear optical crystal ZnTe [15]. A comprehensive study of HMQ-TMS at different pump wavelengths has been performed by Vicario *et al.* [16], generating a maximum achievable bandwidth of up to 15 THz when pumping HMQ-TMS at 1500 nm and 100 Hz repetition-rate. At 1000 nm, Brunner *et al.* have shown the superior performance of HMQ-TMS compared to GaP, with an energy conversion efficiency increase by a factor of 41 [17]. Lastly, Rovere *et al.* have reported the combination of a 500 Hz Yb:KGW bulk laser pumping HMQ-TMS at 1030 nm, producing promising results with a 0.26% conversion efficiency [18]. The potential of this crystal is further highlighted by comparing the electro-optic coefficient for HMQ-TMS at $\sim 50 \text{ pm}\cdot\text{V}^{-1}$ [13,14] to that of GaP at $\sim 1 \text{ pm}\cdot\text{V}^{-1}$ [19,20].

In this work, we show the first application of a 10 MHz Yb:fibre laser system for pumping HMQ-TMS at 1035 nm for THz wave generation through OR. Compared to the commonly used GaP, we show a tenfold electric field increase with a peak on-axis field strength of $7 \text{ kV}\cdot\text{cm}^{-1}$ and an average power of 0.38 mW with a generated spectral bandwidth of up to 6 THz at -30 dB.

2. Theory

For an efficient frequency conversion process within a nonlinear crystal, the pump and newly generated frequencies need to be phase-matched. The physical length of this overlap is termed the coherence length l_c and is given by

$$l_c = \frac{\lambda_{\text{THz}}}{2(n_{\text{THz}} - n_g)}, \quad (1)$$

with the refractive index at the THz wavelength n_{THz} and the group index of the pump wavelength n_g [13]. From Eq. (1) it is clear that the coherence length increases when the refractive index mismatch of pump and THz wavelengths is minimised, allowing for the use of thicker generation crystals and improving conversion efficiencies. The crystal thickness is ultimately limited by dispersive effects acting upon the ultrashort pulse, essentially reducing the peak power of the pump pulse. Sources based on ytterbium active media occupy an operating range around 1030 nm, restricting the choice of nonlinear crystals suitable for THz generation. Figure 1(a) shows the relationship between the coherence length and the optical pump wavelength for GaP, where we consider the optical group index dispersion from [21] and the THz index from [22]. It is clear to see that for pump wavelengths around 1030 nm, a 1 mm thick crystal will support THz wave generation up to nearly 4 THz because the group index of the pump ($n_g = 3.31$) and the refractive index of the THz wave ($n_{\text{THz}} \approx 3.36$) in this wavelength region are relatively well

matched [22]. The nonlinear coefficient of GaP, however, limits the efficiency of the generation process. While organic nonlinear optical crystals offer a higher nonlinear coefficient, the larger mismatch between the optical group index at 1030 nm ($n_g \approx 2.15$) and the refractive index at THz frequencies (ranging from 2.0-2.3 [16,17]) necessitates the use of thinner crystals for efficient and broadband THz wave generation [see Fig. 1(b)].

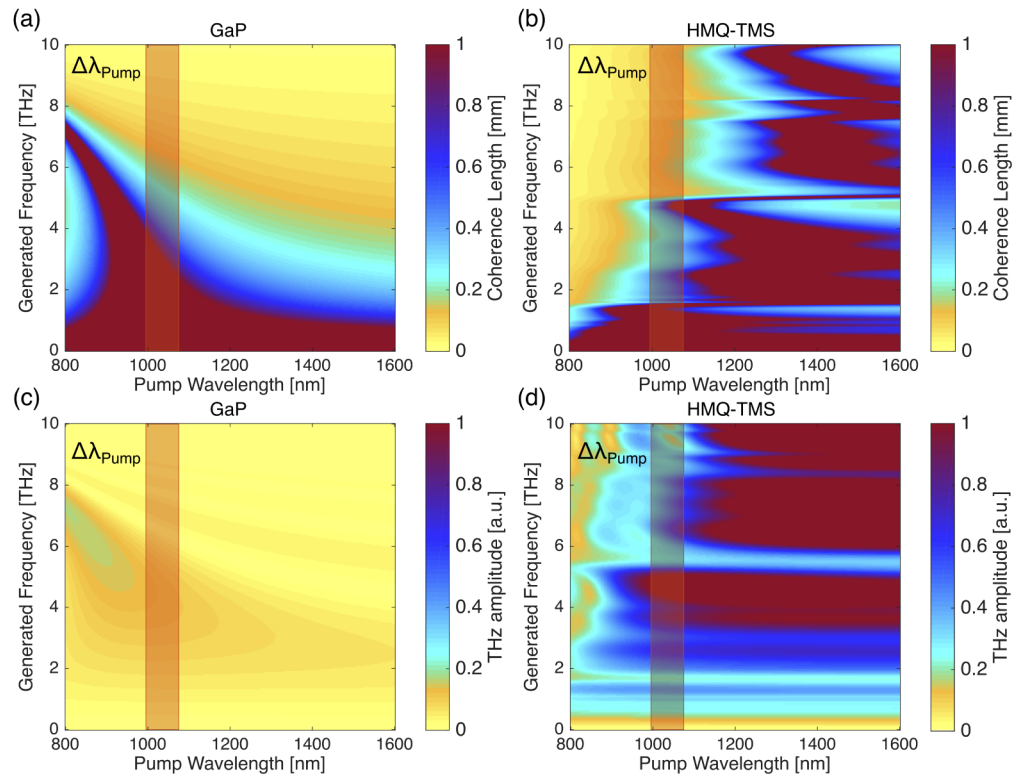


Fig. 1. (a) Coherence length as a function of pump wavelength and the generated THz frequency (the bandwidth of our experimental pump laser spectrum is indicated with an orange shaded area) for GaP and (b) HMQ-TMS. (c) Generated THz spectrum considering 30 fs optical pulses as a function of pump wavelength for 0.25 mm thick GaP and (d) 0.25 mm thick HMQ-TMS.

The trade-off between phase-matching considerations and the magnitude of the materials' nonlinear coefficient on the overall THz wave generation can be modelled using an analytical approach [23]. Here, we adopt a non-depleted, plane-wave pump approximation, account for the frequency dependent Fresnel transmission at each crystal-air interface, assume a transform limited 30 fs input pump and probe pulse, measurement of the generated THz waveform in time using air-biased coherent detection (i.e. a broadband detection scheme that does not impose a spectral response function), and realistic material parameters including the dispersion of the refractive index and absorption in the THz and optical range for GaP [21,22] and for HMQ-TMS [16,17], respectively. It can be seen from Figs. 1(c) and (d), where the generated THz amplitude is plotted as a function of the input pump wavelength for two 0.25 mm thick crystals of GaP and HMQ-TMS, that the potential of HMQ-TMS as a THz emitter compatible with high-power, high-repetition-rate ytterbium-based pump sources is superior to that of GaP by nearly an order of magnitude and supports broader band THz generation.

Using the same model approximation, we have evaluated the generated THz spectra as a function of the input pump pulse duration (Fig. 2) by keeping the pump pulse energy constant. The modelling shows that the output spectral bandwidth scales favourably with a decreasing input pulse duration, showing higher frequency spectral components and an overall higher spectral amplitude compared to the output at longer input pump pulses. For ease of comparison all curves are normalised to the peak of the 30 fs trace. These results emphasise the importance of pulse compression of the pump laser for the generation of efficient broadband THz radiation. We restrict ourselves to a minimum pulse duration of 30 fs because this is compatible with our experimental conditions and the optical parameters of HMQ-TMS at frequencies above 12 THz are poorly defined.

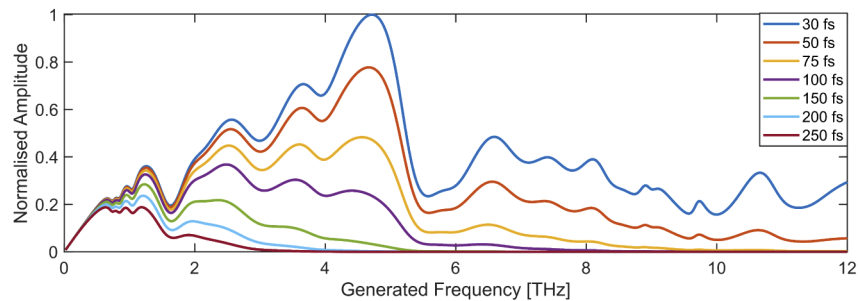


Fig. 2. Behaviour of the THz spectrum for different transform limited pump-pulses centred at 1035 nm at equal pulse energy, normalised to the 30 fs output. The modelling highlights the benefit of using shorter pump-pulses, yielding a larger bandwidth with greater efficiency.

3. Experimental setup

3.1. Pump pulse characterisation

The output of a Yb:fibre laser with a centre wavelength of 1035 nm delivering 250 fs pulses at 10 MHz is coupled into a solid, large-core photonic crystal fibre (LMA-PCF, NKT Photonics) resulting in spectral broadening through self-phase modulation (SPM), which subsequently allows for compression with a pair of SF10 prisms to 30 fs with an output power of 2.5 W. The pump pulse is characterised using frequency-resolved optical gating (FROG, MESA Photonics), shown in Fig. 3. Furthermore, the pulse duration is confirmed to be 30 fs through use of a commercial intensity autocorrelator (APE Berlin) and a home-built interferometric autocorrelator. Figures 3(a) and 3(b) show strong agreement between the measured and retrieved FROG traces, with a residual FROG error of 0.0090, where the FROG error is the root mean square difference between the measured and retrieved traces divided by the number of points in the trace. Figure 3(c) shows the retrieved pulse shape in time, its phase, and a sech^2 fit to the main peak containing $\sim 70\%$ of the pulse energy. The observed satellite pulses are a characteristic of uncompensated higher-order phase contributions arising from the spectral broadening through SPM in the LMA-PCF [24] and residual higher-order dispersion accumulated in the fibre pump laser. The strong SPM manifests itself in Fig. 3(d), where we show the spectrum of the initial pump pulse before spectral broadening and the corresponding broadened pulse spectrum, recorded with an optical spectrum analyser.

3.2. Setup for THz wave generation

Our experimental setup for THz wave generation through OR is shown in Fig. 4(a). A small amount (~ 25 mW) of the power is split and sent to the delay stage, termed the ‘probe’ beam. The remaining power, termed the ‘pump’ beam, is variably attenuated down below 2 W in order

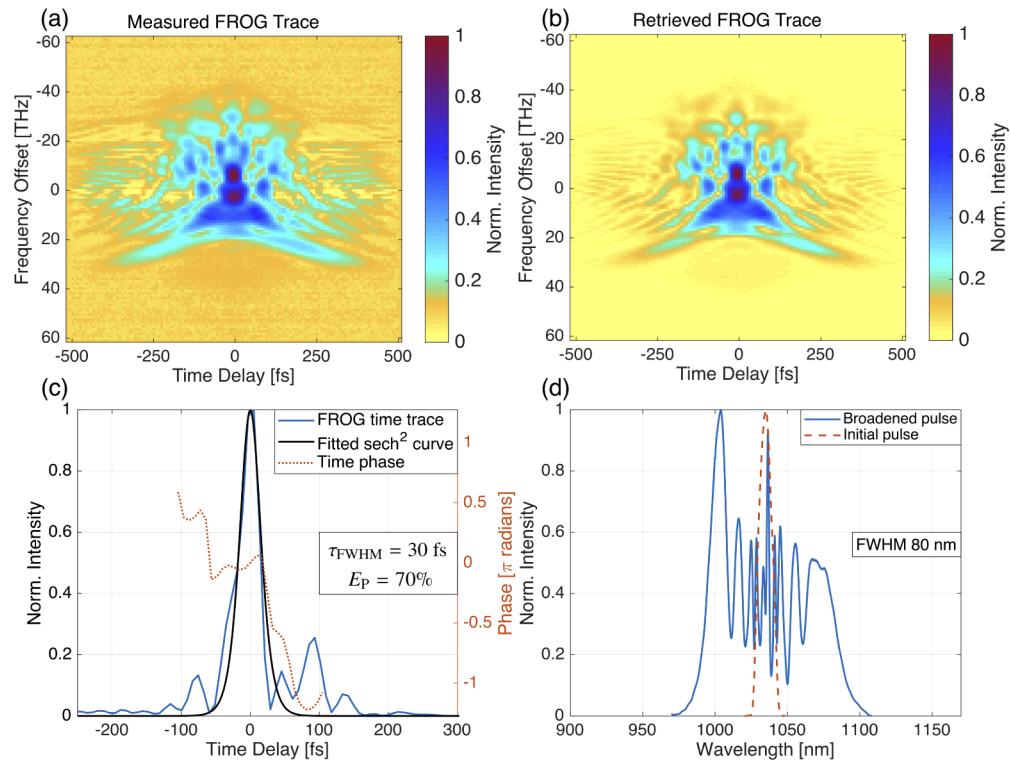


Fig. 3. Pump laser characteristics. (a) Measured FROG trace, (b) retrieved FROG trace, (c) FROG-retrieved time trace, phase and sech²-fit, and (d) the corresponding pulse spectrum.

to avoid optical damage in the generation crystal. The pump beam is focussed with a 150 mm lens to a spot size at $1/e^2$ of ~ 0.1 mm in diameter, which is sub-wavelength for the emitted THz radiation. Hence, this tight-focussing regime yields a strongly divergent THz beam which is not fully captured by the collimating paraboloidal mirror. However, such tight focussing is necessary to achieve the required intensities within the crystal due to the limited pulse energy from the pump laser. We assess THz wave generation in two distinct samples: a 1 mm thick GaP crystal and a 0.25 mm HMQ-TMS sample. Figure 4(b) shows an image of the HMQ-TMS crystal for illustrative purposes. Comparative experiments with 0.3 mm GaP crystals showed similar data with a slightly larger bandwidth. However, since the spectral difference between THz pulses from 1 mm and 0.3 mm GaP is not substantial, we chose to compare a 1 mm GaP to the 0.25 mm HMQ-TMS crystal for practical reasons relating to the generated power and thus ease of detection through electro-optic sampling (EOS). The generation crystal is placed on a translation stage in order to adjust the peak fluence for a given pump power by shifting the crystal in or out of focus. Teflon is used to block the residual near-IR power, but transmit the generated THz radiation, which is then collimated by a 3 inch focal length off-axis paraboloidal mirror. Following this, the THz beam is overlaid with the probe beam from the delay stage and focussed with a 2 inch focal length paraboloidal mirror into a 0.3 mm thick GaP detection crystal for EOS. The electric field of the THz pulse induces a birefringence in the detection crystal, which in turn changes the polarisation of the probe beam. The hereby altered probe beam is then sent through a quarter wave-plate and a Wollaston prism onto a balanced detector, allowing the recording of the THz electric field trace in time with the use of a lock-in amplifier phase-locked to a chopper in the

pump beam at 500 Hz. The beam path between the two crystals is purged with nitrogen to reduce absorption due to water vapour in the ambient atmosphere.

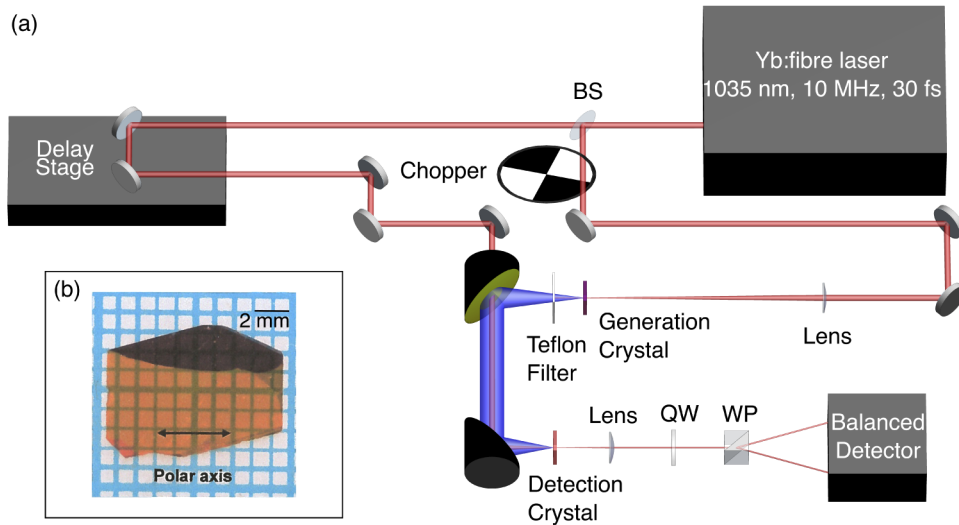


Fig. 4. (a) Overview of the experimental setup, with the generation crystal (1 mm thick GaP / 0.25 mm HMQ-TMS) and detection crystal (0.3 mm thick GaP). BS: Beamsplitter, WP: Wollaston Prism, QW: Quarter Waveplate. (b) Image of the crystal HMQ-TMS.

The generated THz average power is recorded with a calibrated pyro-electric detector (Gentec-EO) positioned in place of the detection crystal. Due to space constraints, the power measurement setup is not purged for power measurements. For accurate measurement of the generated THz power, additional filters are added to the beam path to remove any residual pump-power, consisting of a series of Teflon strips with 0.08 mm thickness (THz transmission 89% each), a low-pass filter in combination with an additional 0.15 mm of Teflon (THz transmission 75%), and a silicon wafer at 0.54 mm thickness (THz transmission 47%). The atmospheric THz transmission through free space for this setup is 61%. Filter transmission values are recorded with an in-house broadband THz system (reaching 30 THz [25]) and extracted for the relevant spectral range of 0.5-5 THz (for HMQ-TMS) and 0.5-3.5 THz (for GaP), rather than applying standard literature values for each material, as batch-to-batch thickness, production quality, and individual assembly of the filters will have an effect on the absolute transmission and the ultimate calibration accuracy. These spectral windows were chosen based on the -20 dB value of the bandwidth for the respective crystals. Furthermore, the use of stacked silicon wafers was avoided, since the transmission function is sensitive to the angular alignment of consecutive wafers and is not given by the simple approximation of 0.5^n [26]. As a final step of proof, a single silicon wafer is temporarily held directly in front of the detector to verify a $\sim 50\%$ decrease in power, in order to rule out the presence of any residual near-IR or stray light.

4. Results and discussion

4.1. Electro-optic sampling

The resulting THz field traces of 1 mm GaP and 0.25 mm HMQ-TMS are shown in Fig. 5(a). Under equal experimental conditions, the HMQ-TMS shows an electric field amplitude more than ten times stronger than that generated through GaP, with a transient duration (leading maximum to minimum) of 150 fs. This order of magnitude increase of the THz field is in line with previous work comparing GaP to HMQ-TMS [17] at 1000 nm. Furthermore, as can be seen in the inset

of Fig. 5(a), because of our compressed ultrashort probe pulse of 30 fs, we can probe the EOS signal with high temporal resolution.

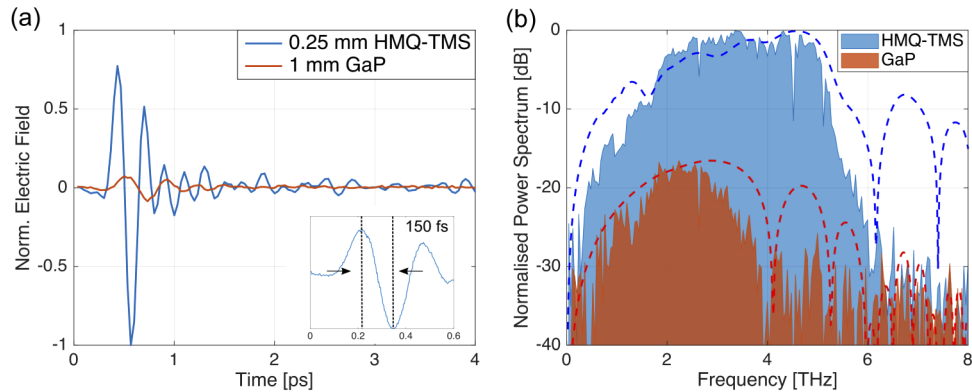


Fig. 5. (a) Normalised time trace of the generated THz field acquired through EOS for 0.25 mm thick HMQ-TMS (blue) and 1 mm thick GaP (red) at equivalent laboratory settings, showing a tenfold increase of field amplitude for HMQ-TMS over GaP and a short transient duration of 150 fs. (b) Spectrum of HMQ-TMS (shaded blue) and GaP (shaded red) normalised to the HMQ-TMS trace, with analytical modelling of expected bandwidths for a transform limited 30 fs pump pulse for HMQ-TMS (dotted red) and GaP (dotted blue).

Figure 5(b) shows the generated THz spectrum in GaP compared with that of HMQ-TMS, normalised to the peak of the HMQ-TMS spectrum (shaded areas). In addition, we plot the calculated THz spectra based on our analytic model (dashed lines) using realistic experimental parameters, including the spectral response function of the 0.3 mm thick GaP detection crystal and the spectrally dependent transmission of the Teflon filter that both impose a high-frequency cut-off. For this evaluation we also consider the finite diameter of the tightly focussed pump pulses on the crystal instead of the plane-wave approximation following the model in [23]. Apart from the almost 100 times larger spectral power (consistent with previous reports comparing HMQ-TMS against GaP [17]), we also observe a significant improvement in the spectral bandwidth up to 6 THz at -30 dB for HMQ-TMS – almost twice the bandwidth we achieve with GaP. The overall spectral shape of the HMQ-TMS and the GaP is well reproduced by our modelling for low frequencies. In both cases, however, the high-frequency content present in the model is not faithfully reproduced in the experiment. We attribute this to the presence of low-level temporal satellites persistent in our experimental pump pulses that arise from uncompensated higher-order spectral phase components, observed experimentally in our FROG measurements of the near-IR pump pulses after compression (see Fig. 3). It should be noted that the thinner GaP crystal (0.3 mm) yields a slightly larger bandwidth exceeding 4 THz, although at the cost of reduced THz power. This is in agreement with earlier reports that show a bandwidth up to 7 THz with a 0.15 mm GaP at 1030 nm [27], although with a notable shift of the spectrum to higher frequencies overall, and a bandwidth of 8 THz with 0.4 mm GaP at 800 nm pump wavelength [10]. Our HMQ-TMS spectrum shows a smooth, almost gap-less, flat-top shape from 2 to 5 THz (in a nitrogen purged atmosphere), advantageous for diverse applications not only in spectroscopy; previous work on 0.22 mm HMQ-TMS with 65 fs pump pulses at 1000 nm centre wavelength showed a bandwidth up to ~5 THz [16]. Our experimental approach proves, in addition to our modelling, that a shorter pump pulse (and consequently a larger pump bandwidth) generates a broader THz spectrum, emphasising the utilisation of enhanced pulse compression schemes for broadband THz generation. Furthermore, our modelling based on transform-limited input pulses underlines the need for high-quality pulse compression to maximise the achievable bandwidth.

4.2. Conversion efficiency and power

We record a maximum THz output power with GaP of 8.8 μW when pumped at 2 W (0.2 μJ), yielding a conversion efficiency of 4.0×10^{-6} . This is in the range of other reported values for GaP pumped at similar wavelengths, being 10 μW (repetition-rate: 61 MHz, pump pulse duration: 50 fs), efficiency on the order of 2.5×10^{-6} [22]; 1.5 μW (repetition-rate: 78 MHz, pump pulse duration: 20 fs), efficiency 0.3×10^{-6} [11]; and 1.35 mW (repetition-rate: 13.4 MHz, pump pulse duration: 88 fs), efficiency 1.2×10^{-5} [9]. Spot size, pump pulse duration and power, and crystal quality affect the conversion process of OR, leading to the slight discrepancies shown here.

With the HMQ-TMS crystal, the collected THz output power when pumped at 700 mW (70 nJ) is 53 μW , with a power efficiency of 7.6×10^{-5} . At 2 W (0.2 μJ) pump power and a larger spot size, 380 μW and a conversion efficiency of 1.86×10^{-4} is reached. This is a significant improvement over GaP, potentially allowing for multi-mW level THz sources through shorter pump pulses and larger pump powers together with a looser focus; mW-level THz powers could be reached with just ~ 4 W (0.4 μJ) of pump power at 10 MHz repetition-rate – scaling the THz power using large-area emitters will be the subject of future studies. Previous work has reached conversion efficiencies of 26×10^{-4} at 500 Hz and 1030 nm in a 0.63 mm HMQ-TMS [18], 3.5×10^{-5} at 800 nm [15], and 4.9×10^{-4} for a 0.66 mm thick HMQ-TMS at 1300 nm. Those results indicate a power efficiency increase of two orders of magnitude compared to inorganic crystals under equal circumstances, which is expected from the tenfold field-increase.

4.3. Thermal damage threshold

HMQ-TMS has been tested for damage at low repetition-rates, yielding an upper limit on the pump fluence of $>20 \text{ mJ}\cdot\text{cm}^{-2}$ at 100 Hz [16]. Considering this and other previous work [18], as well as our experience with GaP (damage threshold of $4.3 \text{ mJ}\cdot\text{cm}^{-2}$ at 52 MHz [28]), we set our average power to 1 W (0.1 μJ) at a spot size diameter of 0.10 mm, resulting in a fluence of $\sim 2.5 \text{ mJ}\cdot\text{cm}^{-2}$, in order to be well below previously reported damage thresholds. However, due to the elevated repetition-rate, the dominant damage mechanism becomes thermal at a lower fluence rather than being driven by the high peak intensities of low-repetition-rate ultrashort pulse sources. The accumulated heat deposited during the experiment results in a large area of irreversible damage of the crystal at the focus, due to melting (this characteristic is reproducible across multiple HMQ-TMS samples). In order to determine the power-limit for the crystal, the threshold was recorded for varying spot sizes. A range of uncertainty on the damage thresholds results from the spatial properties of the beam-profiler and the crystal-mount not having reversible symmetry. This means, that the measured spot size with the beam-profiler does not necessarily coincide with the spot size in the crystal when placing the translation stage to the same position. Taking this into account, we have determined that the damage threshold for HMQ-TMS at MHz repetition-rates lies between a peak intensity of 52-107 $\text{GW}\cdot\text{cm}^{-2}$ or a fluence range of 1.8-3.6 $\text{mJ}\cdot\text{cm}^{-2}$, with a $1/e^2$ spot diameter $2w$ between 100-70 μm . Peak power was calculated using a pre-factor of 0.88 to compensate for the sech² temporal shape of the pulse, while the peak intensity based on a Gaussian spatial profile was calculated using $I_{\text{peak}} = 2 \cdot P_{\text{peak}} / (\pi w^2)$. These updated damage thresholds are significantly lower than previously reported for the kHz regime. The reduced damage threshold for high repetition-rate systems is in agreement with literature data available for GaP [28]. When operating at high powers, but below the damage threshold, over the course of our experimental campaign, with several illumination periods exceeding two hours, the HMQ-TMS crystals showed no measurable signs of degradation or drop in performance. Possible long term degradation due to exposure to ambient conditions was avoided by storing the samples in a nitrogen-purged environment between experiments.

4.4. Proof-of-concept, spot size and field strength

In order to verify the operability of the HMQ-TMS THz source, a standard time-domain spectroscopy (TDS) measurement is conducted on a high resistivity (HR) silicon wafer. First, a reference time trace of the HMQ-TMS THz signal is recorded through the EOS method. Following this, under equal conditions, a time trace with the silicon wafer placed into the THz beam path is recorded as the sample data. With a single THz TDS measurement, we acquire information on the refractive index and absorption coefficient of the sample. Figure 6(a) shows the resulting frequency dependent refractive index retrieved from the experimental data, with the refractive index of 3.46 matching closely literature values for silicon of 3.41 [29]. The discrepancy in the measured and literature values can be accounted for by the uncertainty of the sample thickness. The bandwidth of the HMQ-TMS source, extending up to ~ 6 THz, defines the upper frequency limit on the validity of the refractive index data. This proof-of-concept TDS measurement using our high repetition-rate HMQ-TMS-based THz source pumped by a Yb:fibre laser demonstrates the feasibility of our approach, with overall measurement times reduced compared to low repetition-rate sources. The integration time (or time constant) of the lock-in amplifier is selected to be longer than a minimum value of 100 ms. Shorter integration times and consequently faster data acquisition yield a noisy spectroscopic signal with reduced SNR due to intrinsic source instabilities.

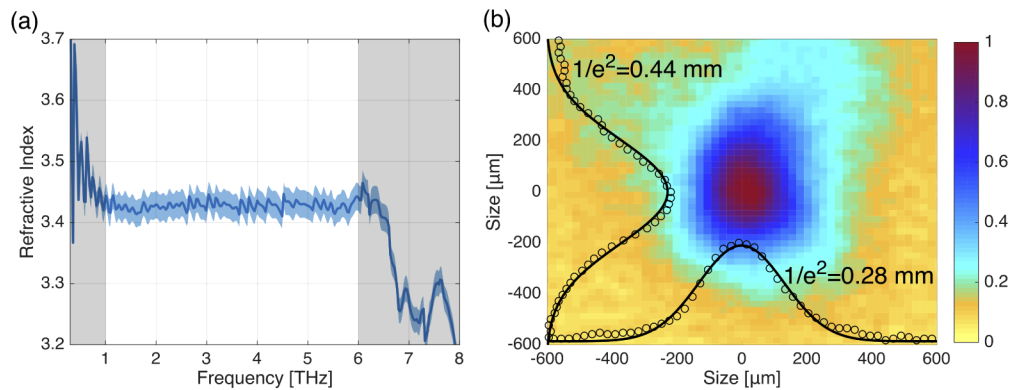


Fig. 6. (a) Retrieved refractive index of a 525 μm thick, high resistivity, polished silicon sample over a 8.5 ps time window. The refractive index matches the literature value of 3.41 within the sample thickness uncertainty of $\pm 1\%$ (blue shaded area). The frequency range with insufficient signal strength and subsequently unreliable data is greyed out. (b) The focussed THz spot size at the position of the detection crystal in the EOS setup measured by a micro-bolometer, with an overlay of Gaussian fits and the $1/e^2$ spot radius values.

Lastly, the focussed spot size of the THz beam from the HMQ-TMS crystal is measured using an uncooled micro-bolometer from NEC (THz Imager IR/V-T0831) with a pixel size of 25.5 μm . The slight ellipticity in the measured THz focus seen in Fig. 6(b) can be attributed to the alignment and focussing characteristics of the paraboloidal mirror leading to an elongation in the vertical (y) dimension. The peak on-axis THz field strength is calculated by taking the measured spatial intensity, which can be expressed as $I(x, y, t) = I_0(t) \exp\left(-\frac{2x^2}{w_x^2} - \frac{2y^2}{w_y^2}\right)$, defined with the $1/e^2$ spot radius w . The THz pulse energy U is obtained from a direct measurement of the THz power and knowledge of the repetition rate, and corresponds to the integral of the instantaneous intensity in time and space $U = \int_{-\infty}^{\infty} dx \int_{-\infty}^{\infty} dy \int_0^T I(x, y, t) dt$. The raw EOS trace $E_{\text{raw}}(t)$ can then

be transformed to an absolute field strength using $I \propto E^2$ and the scaling factor

$$\Gamma = \sqrt{\frac{P}{f_{\text{rep}} c \epsilon_0 \frac{\pi}{2} w_x w_y \int_0^T |E_{\text{raw}}(t)|^2 dt}}. \quad (2)$$

The peak on-axis field strength is found to be $\sim 7 \text{ kV}\cdot\text{cm}^{-1}$, based on a collected average THz power of $P = 0.38 \text{ mW}$ for an input pump power of 2 W at a repetition-rate $f_{\text{rep}} = 10 \text{ MHz}$, with a focussed Gaussian waist radius at $1/e^2$ of $w_x = 278 \text{ }\mu\text{m}$ and $w_y = 439 \text{ }\mu\text{m}$ (and where $c = 2.99 \times 10^8 \text{ m}\cdot\text{s}^{-1}$ is the speed of light in vacuum and $\epsilon_0 = 8.85 \text{ pF}\cdot\text{m}^{-1}$ is vacuum permittivity).

5. Conclusion

We have demonstrated sub-mW THz wave generation at MHz repetition-rates in the organic crystal HMQ-TMS and compared this performance with GaP, showing an efficiency increase by two orders of magnitude when pumped by the spectrally broadened and temporally compressed output of a femtosecond fibre laser at 1035 nm. At 2 W ($0.2 \text{ }\mu\text{J}$) of pump power in a tight focus geometry we generate 0.38 mW of THz power in a 0.25 mm thick HMQ-TMS crystal with an on-axis field strength of $7 \text{ kV}\cdot\text{cm}^{-1}$. Given that HMQ-TMS crystals can be produced with cm^2 areas, further power scaling in excess of 1 mW can be achieved by increasing the available pump power and a loosening of the focus spot to prevent irreversible damage. Furthermore, cleaner compression of the ultrashort pump pulses, with their accompanied large bandwidth, supports broadband THz wave generation beyond 6 THz , though with strong characteristic phonon resonances. We also revise the thermal damage limits of this nonlinear optical crystal at MHz repetition-rates, reporting a reduction at the elevated repetition-rate to a fluence range of $1.8\text{--}3.6 \text{ mJ}\cdot\text{cm}^{-2}$. As a proof-of-principle, we perform a simple THz TDS measurement on a float-zone HR silicon wafer, recovering the refractive index with high accuracy comparable to literature values. We anticipate that our broadband, high-power THz source will be well suited to sensitive spectroscopic applications, where samples with low interaction cross-sections demand measurements performed at high-repetition-rates.

Funding

National Research Foundation of Korea (2014R1A5A1009799, 2019R1A2C3003504); Ministry of Science and ICT, South Korea.

Acknowledgements

We thank Qian Shen for assistance with characterisation of the THz transmission of different materials and Daena Madhi for the use of codes to interface the EOS setup.

Disclosures

The authors declare no conflicts of interest.

References

1. E. Pickwell and V. P. Wallace, "Biomedical applications of terahertz technology," *J. Phys. D: Appl. Phys.* **39**(17), R301–R310 (2006).
2. M. J. Fitch, M. R. Leahy-Hoppa, E. W. Ott, and R. Oslander, "Molecular absorption cross-section and absolute absorptivity in the THz frequency range for the explosives TNT, RDX, HMX, and PETN," *Chem. Phys. Lett.* **443**(4-6), 284–288 (2007).
3. P. Y. Han, M. Tani, M. Usami, S. Kono, R. Kersting, and X. C. Zhang, "A direct comparison between terahertz time-domain spectroscopy and far-infrared Fourier transform spectroscopy," *J. Appl. Phys.* **89**(4), 2357–2359 (2001).
4. K. Sakai, *Terahertz Optoelectronics* (Springer, Berlin, Heidelberg, 2005).
5. J. A. Fueloep, S. Tzortzakakis, and T. Kampfrath, "Laser-Driven Strong-Field Terahertz Sources," *Adv. Opt. Mater.* **8**(3), 1900681 (2020).

6. T. Seifert, S. Jaiswal, U. Martens, J. Hannegan, L. Braun, P. Maldonado, F. Freimuth, A. Kronenberg, J. Henrzi, I. Radu, E. Beaurepaire, Y. Mokrousov, P. M. Oppeneer, M. Jourdan, G. Jakob, D. Turchinovich, L. M. Hayden, M. Wolf, M. Münzenberg, M. Kläui, and T. Kampfrath, "Efficient metallic spintronic emitters of ultrabroadband terahertz radiation," *Nat. Photonics* **10**(7), 483–488 (2016).
7. S. L. Dexheimer, *Terahertz spectroscopy: Principles and applications* (CRC Press, 2017).
8. J. Li, L. Chai, J. Shi, F. Liu, B. Liu, B. Xu, M. Hu, Y. Li, Q. Xing, C. Wang, A. B. Fedotov, and A. M. Zheltikov, "Generation of 0.3 mW high-power broadband terahertz pulses from GaP crystal pumped by negatively chirped femtosecond laser pulses," *Laser Phys. Lett.* **10**(12), 125404 (2013).
9. F. Meyer, N. Hekmat, T. Vogel, A. Omar, S. Mansourzadeh, F. Fobbe, M. Hoffmann, Y. Wang, and C. J. Saraceno, "Milliwatt-Class MHz Repetition-Rate THz Source Driven by a sub-100 fs High Power Thin-Disk Laser," *Int. Conf. IRMMW-THz* **21**, 1–3 (2019).
10. I. D. Vugmeyster, J. F. Whitaker, and R. Merlin, "GaP based terahertz time-domain spectrometer optimized for the 5–8 THz range," *Appl. Phys. Lett.* **101**(18), 181101 (2012).
11. I. Pupeza, C. Hofer, N. Lilienfein, B. Globisch, N. Karpowicz, J. Xu, and T. Butler, "Three-octave terahertz pulses from optical rectification of 20 fs, 1 μm , 78 MHz pulses in GaP," *J. Phys. B: At. Mol. Opt. Phys.* **51**(15), 154002 (2018).
12. M. C. Hoffmann, K. L. Yeh, H. Y. Hwang, T. S. Sosnowski, B. S. Prall, J. Hebling, and K. A. Nelson, "Fiber laser pumped high average power single-cycle terahertz pulse source," *Appl. Phys. Lett.* **93**(14), 141107 (2008).
13. M. Jazbinsek, U. Puc, A. Abina, and A. Zidansek, "Organic Crystals for THz Photonics," *Appl. Sci.* **9**(5), 882 (2019).
14. J. H. Jeong, B. J. Kang, J. S. Kim, M. Jazbinsek, S. H. Lee, S. C. Lee, I. H. Baek, H. Yun, J. Kim, Y. S. Lee, J. H. Lee, J. H. Kim, F. Rotermund, and O. P. Kwon, "High-power broadband organic THz generator," *Sci. Rep.* **3**(1), 3200 (2013).
15. J. Lu, H. Y. Hwang, X. Li, S.-H. Lee, O.-P. Kwon, and K. A. Nelson, "Tunable multi-cycle THz generation in organic crystal HMQ-TMS," *Opt. Express* **23**(17), 22723–22729 (2015).
16. C. Vicario, B. Monoszlai, M. Jazbinsek, S. H. Lee, O. P. Kwon, and C. P. Hauri, "Intense, carrier frequency and bandwidth tunable quasi single-cycle pulses from an organic emitter covering the Terahertz frequency gap," *Sci. Rep.* **5**(1), 14394 (2015).
17. F. D. J. Brunner, S.-H. Lee, O.-P. Kwon, and T. Feurer, "THz generation by optical rectification of near-infrared laser pulses in the organic nonlinear optical crystal HMQ-TMS," *Opt. Mater. Express* **4**(8), 1586 (2014).
18. A. Rovere, Y.-G. Jeong, R. Piccoli, S.-H. Lee, S.-C. Lee, O.-P. Kwon, M. Jazbinsek, R. Morandotti, and L. Razzari, "Generation of high-field terahertz pulses in an HMQ-TMS organic crystal pumped by an ytterbium laser at 1030 nm," *Opt. Express* **26**(3), 2509 (2018).
19. D. F. Nelson and E. H. Turner, "Electro-optic and piezoelectric coefficients and refractive index of gallium phosphide," *J. Appl. Phys.* **39**(7), 3337–3343 (1968).
20. J. Lu, S.-H. Lee, X. Li, S.-C. Lee, J.-H. Han, O.-P. Kwon, and K. A. Nelson, "Efficient terahertz generation in highly nonlinear organic crystal HMB-TMS," *Opt. Express* **26**(23), 30786 (2018).
21. S. Casalbuoni, H. Scharb, B. Schmidt, P. Schmuesser, B. Steffen, and A. Winter, "Numerical studies on the electro-optic detection of femtosecond electron bunches," *Phys. Rev. Spec. Top.–Accel. Beams* **11**(7), 072802 (2008).
22. C. Paradis, J. Drs, N. Modsching, O. Razskazovskaya, F. Meyer, C. Kränkel, C. J. Saraceno, V. J. Wittwer, and T. Südmeyer, "Broadband terahertz pulse generation driven by an ultrafast thin-disk laser oscillator," *Opt. Express* **26**(20), 26377 (2018).
23. A. Schneider, M. Neis, M. Stillhart, B. Ruiz, R. U. A. Khan, and P. Günter, "Generation of terahertz pulses through optical rectification in organic DAST crystals: theory and experiment," *J. Opt. Soc. Am. B* **23**(9), 1822–1835 (2006).
24. G. P. Agrawal, *Applications of Nonlinear Fiber Optics* (Academic Press, 2008).
25. A. T. Tarekne, B. Zhou, K. Kaltenecker, K. Iwaszczuk, S. Clark, and P. U. Jepsen, "Terahertz time-domain spectroscopy of zone-folded acoustic phonons in 4H and 6H silicon carbide," *Opt. Express* **27**(3), 3618 (2019).
26. K. J. Kaltenecker, E. J. Kelleher, B. Zhou, and P. U. Jepsen, "Attenuation of THz Beams: A "How to" Tutorial," *J. Infrared, Millimeter, Terahertz Waves* **40**(8), 878–904 (2019).
27. J. Drs, N. Modsching, C. Paradis, C. Kränkel, V. J. Wittwer, O. Razskazovskaya, and T. Südmeyer, "New horizons for high power broadband THz sources driven by ultrafast Yb-based thin-disk laser oscillators," *CLEO STh3F.5*, (2019).
28. Y. Li, F. Liu, Y. Li, L. Chai, Q. Xing, M. Hu, and C. Wang, "Experimental study on GaP surface damage threshold induced by a high repetition rate femtosecond laser," *Appl. Opt.* **50**(13), 1958–1962 (2011).
29. J. Dai, J. Zhang, W. Zhang, and D. Grischkowsky, "Terahertz time-domain spectroscopy characterization of the far-infrared absorption and index of refraction of high-resistivity, float-zone silicon," *J. Opt. Soc. Am. B* **21**(7), 1379–1386 (2004).